Oil & Gas Science and Technology – Rev. IFP, Vol. 64 (2009), No. 6, pp. 697-706

DOI: 10.2516/ogst/2009021

Dossier

Catalysts and Adsorbents: from Molecular Insight to Industrial Optimization
Catalyseurs et adsorbants : de la compréhension moléculaire à l'optimisation industrielle

Nanostructured Heterogeneous Catalysts: Well Defined Platinum Nanoparticles Supported on Alumina.

Preparation, Characterization and Application to the Selective Hydrogenation of Buta-1,3-diene

D. Pham Minh, Y. Oudart, B. Baubet, C. Verdon and C. Thomazeau

Institut français du pétrole, IFP-Lyon, Direction Catalyse & Séparation, BP 3, 69390 Vernaison - France
e-mail: doanhoa2000@yahoo.fr - yohan.oudart@ifp.fr - bertrand.baubet@wanadoo.fr - catherine.verdon@ifp.fr - cecile.thomazeau@ifp.fr

Résumé — Catalyseurs hétérogènes nanostructurés : nanoparticules de platine de morphologies définies supportées sur alumine. Préparation, caractérisation et application en hydrogénation sélective du buta-1,3-diène — Des nanoparticules de platine possédant des morphologies particulières ont été préparées en solution aqueuse. Des paramètres clefs, tels que le ratio entre le tensioactif (bromure de cetyltrimethylammonium, CTAB) et le précurseur de platine (H_2PtCl_6), la température, l'atmosphère (argon ou hydrogène), doivent être maîtrisés pour contrôler la formation des particules de platine nanostructurées et leurs morphologies. Des nanoparticules de platine se présentant soit sous la forme de cubes, soit sous la forme d'un mélange de formes (bâtonnets, cubes, tétraèdres), soit sous la forme de polyèdres ont ainsi été obtenues selon le ratio CTAB/Pt utilisé, l'atmosphère et la température. Un mécanisme de formation de ces nanoparticules de platine est proposé. Les nanoparticules de platine ont ensuite été déposées sur alumine et leurs propriétés catalytiques évaluées dans la réaction d'hydrogénation sélective du buta-1,3-diene. Les catalyseurs préparés avec des nanoparticules de platine se présentant sous la forme de polyèdres, qui exposent préférentiellement les plans cristallographiques (111), sont les plus sélectifs pour l'hydrogénation du buta-1,3-diene en butènes, avec une diminution considérable de l'hydrogénation complète vers les butanes.

Abstract — Nanostructured Heterogeneous Catalysts: Well Defined Platinum Nanoparticles Supported on Alumina. Preparation, Characterization and Application to the Selective Hydrogenation of Buta-1,3-diene — *Platinum nanoparticles with specific morphologies were prepared in aqueous solution. Key parameters, such as cationic surfactant (cetyltrimethylammonium bromide CTAB) and platinum precursor* (H_2PtCl_6) *ratio, temperature, atmosphere (argon or hydrogen), were required to control the formation of nanostructured platinum particles, with well defined morphologies, and even to control their morphology. Platinum nanoparticles with mainly cubic morphologies, with a mix of morphologies (rods, cubes, tetrahedra) or with mainly polyhedric morphologies, were thus obtained depending on CTAB/Pt ratio, atmosphere and temperature. A mechanism of formation of theses platinum nanoparticles was proposed using a time resolved transmission electron microscopy study. After deposition onto* Al_2O_3, *the well crystallized nanostructured platinum particles were evaluated in the selective hydrogenation of buta-1,3-diene. Catalysts prepared with platinum nanoparticles exposing mainly the (111) crystallographic plane (polyhedric morphologies) were the most selective for the selective hydrogenation of buta-1,3-diene into butenes with a drastic decreasing of further hydrogenation into n-butane.*

INTRODUCTION

Over the last decade, a growing interest for nanostructured materials and nanoparticles – with dimensions in the nanometric range – has induced an important research effort, mainly focused on synthesis and characterization of well structured inorganic and metallic nanoparticles. It is now well known that for such nanoparticles, interesting physical properties such as optical and electronic effects can be observed because the mean free path of electrons in the metal and the particle size become comparable [1]. A new challenging task is now to control the shape of such nanoparticles since it is possible to correlate physical properties with the shape of a metallic nanoparticle, mainly for optical applications [2]. For instance, nanorods of Ag can present a red-shift of their longitudinal plasmon band with increasing aspect ratio [3]. Another example is the enhanced SERS effect of anisotropic nanoparticles of Au or Ag compared to spherical ones [4]. From a catalytic point of view, the use of nanoparticles with particular shapes (rods, cubes, tetrahedra, etc.) induces a precise control of their surface structure: type of exposed crystallographic planes, proportion between atoms on corners, edges or facets, thus giving the possibility to tune the activity and/or the selectivity of a catalytic system [5] for a given reaction. As a result, catalysis research efforts which were until today essentially focused on dispersion and particles size effects studies are now dealing with nanoparticles owning specific morphologies and showing preferential crystallographic planes. It has been established, for a set of various reactions, water gas shift [6], hydrogenation [7, 8], oxidation [9] as well as reduction [10] reactions that both activity and selectivity are highly dependent on the morphology and therefore on the exposed crystallographic planes on nanoparticles surfaces.

For these reasons, efforts have been devoted to the preparation of metallic nanoparticles with well defined morphologies. In general, such syntheses involve the reduction of a metallic salt precursor using a reducing agent, in the presence of a stabilizer. The stabilizer could be an ion, a surfactant, a ligand or a polymer and is adsorbed on specific crystallographic planes. Since the crystalline growth rate varies exponentially with the surface energy, the selective adsorption of an additive on a given crystallographic plane can inhibit the growth rate along one crystallographic direction leading to a preferential growth along one other specific direction. This thermodynamic control was successfully applied in nanostructured metallic particles synthesis in organic solution (polyol processes) [11, 12] using a polymer as a capping agent, or in aqueous solution using a surfactant as both a capping and a structure-directing agent, as it was previously done for Au [13] or Pd [14, 15]. Platinum nanoparticles can be synthesized in aqueous solutions using a number of different methods. A high proportion of well-defined platinum nanoparticles (cubes 64%), exposing mainly the (100) crystallographic plane, was successfully synthesized in aqueous solution using N-isopropylacrylamide (NIPA) [16] as a capping agent, hydrogen as a reducer and K_2PtCl_4 as a platinum precursor. Cubes, exposing mainly the (100) crystallographic plane, or tetrahedra, exposing mainly the (111) crystallographic plane [17], were also obtained using sodium polyacrylate (PASO). The variation of the PASO/Pt ratio between 1 and 5 leads to a majority of cubes (between 60% and 80%, PASO/Pt = 1) or to a majority of tetrahedra (60%, PASO/Pt = 5). The proportion of cubes could be even greater (until 80%) using polyacrylic acid sodium salt (PAA) and NaI as an additive [18]. Tetrahedra were also obtained using polyvinylpyrrolydone (PVP), adjusting the pH permitted to form up to 75% of tetrahedra [19, 20]. Platinum nanoparticules with well defined morphologies were obtained using citrate as a structure directing agent [21, 22]. So, without or with low amounts of citrate, cubes and truncated octahedra were observed and when the proportion of citrate was raised, the proportion of tetrahedra was increased. Other reducers such as alcohols were also used. Very narrow particle size distributions, included in the range 1-3 nm could be obtained but shapes of platinum nanoparticles could not be controlled [23-25]. So, many methods have been developed to synthesize platinum nanoparticles in aqueous solution. Nevertheless, yields were never mentioned or when indications (coloration of solutions) were given, they suggested poor ones. This was essentially due to the use of too weak reducing agents to reduce the platinum precursor salt. Consequently, strong reducing agents such as sodium borohydride were also used and structured platinum nanoparticles such as cubes or cuboctahedra [26-28] could be obtained. Nevertheless, the required quantities of sodium borohydride were relatively high, with $NaBH_4$/Pt ratios until 40.

The relationship between the exposed crystallographic plane and the catalytic properties has been previously demonstrated on extended single crystals for platinum [29] for cyclohexene hydrogenation. For buta-1,3-diene hydrogenation, higher activities were reported for the (110) crystallographic plane compared to the (111) crystallographic plane of platinum single crystals [30]. The relationship between platinum nanoparticules morphology and catalytic properties has also been established for a set of catalytic reactions for platinum nanoparticles. For NO reduction by methane [16], both the size and the dominant crystallographic orientation of platinum nanoparticles have been found to be determining factors for catalyst activity and selectivity, with unusual selectivities observed for cubic platinum nanoparticles. For electron-transfer reaction in solution, it has been shown that average rate constants and activation energies are function of platinum nanoparticles shape with the highest rate constant measured on tetrahedral platinum nanoparticles [31]. The influence of platinum nanoparticles surface structure on the selective hydrogenation of α, β

unsaturated aldehydes has also been studied. Catalytic performances showed a strong structure sensitive character with the highest activity measured on (100) preferentially oriented platinum nanoparticles and the highest selectivity towards unsaturated alcohol measured on (111) preferentially oriented platinum nanoparticles [32]. For benzene hydrogenation, the catalytic selectivity was also strongly affected by platinum nanoparticle shape when performances of cubic platinum nanoparticles were compared to cuboctahedral ones [33].

The objective of the present study is to apply the approach previously used for the synthesis of palladium nanostructured nanoparticles to the preparation of well defined platinum nanoparticles in aqueous solution. Nanoparticles with morphologies exposing mainly the (100) crystallographic plane or mainly the (111) crystallographic plane are prepared selectively with a precise control of the experimental conditions of synthesis. A mechanism of formation of theses platinum nanoparticles is proposed. The relationship between the exposed crystallographic plane and selectivity is studied for the selective hydrogenation of buta-1,3-diene.

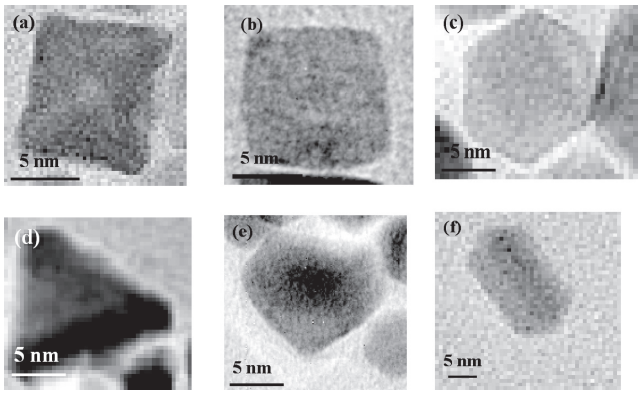

Figure 1

2D-TEM characterization of each type of platinum nanoparticle: a) pseudo-cube; b) cube; c) polyhedron; d) tetrahedron; e) cubooctahedron; f) rod.

1 EXPERIMENTAL SECTION

1.1 Synthesis of Different Platinum Nanostructures

All the preparations were performed under argon atmosphere using a standard vacuum line apparatus. Before use, deionised water was deoxygenized by 20 minutes vigorous argon bubbling. The hexachloroplatinic solution (H_2PtCl_6) was aged at least two days before use. Platinum nanoparticles were then deposited onto a macroporous γ-alumina support (S_{BET} = 140 m^2/g).

1.1.1 Preparation of Platinum Nanoparticles

37.5 mL of an aqueous of (7.5-90 mM) CTAB (cetyltrimethyl-ammonium bromide) heated 10 minutes at (50-70°C) were added to 18.4 mL of an aqueous 3 mM H_2PtCl_6 solution under gently stirring at (50-70°C). In the *Pt-polyhedron*$_{Sol}$ synthesis, argon was replaced by dihydrogen during 10 minutes. Then, injections of 0.3 mL of a (9.9-15.7 mM) $NaBH_4$ solution were made every minute during 15 minutes. The solution colour moved from bright yellow to black in few seconds during those sequential injections. The gentle stirring was then stopped and the solution aged three hours at (50-70°C). Platinum nanoparticles with different morphologies distributions were obtained depending on the experimental conditions of synthesis *(Tab. 1, Fig. 1, 2)*. The characterized samples of platinum nanoparticules in solution are labelled as Pt-(predominant morphology)$_{Sol}$.

1.1.2 Preparation of Supported Platinum Nanoparticles

3.6 g of alumina were added to solutions after ageing, and stirred during two hours. After filtration, the solid was dried overnight at 30°C. The corresponding catalysts prepared by deposition of platinum nanoparticles solutions on alumina are labelled as Pt-(predominant morphology)$_{Cat}$.

1.1.3 Preparation of a Reference Catalyst

A reference catalyst, *Pt-Ref*$_{Cat}$ (0.3% weight Pt) containing platinum nanoparticles without any specific morphologies

TABLE 1

Shapes frequencies of structured platinum nanoparticles deduced from TEM for each set of experimental conditions for platinum nanoparticles synthesis

Sample	Proportion in each morphology deduced from TEM									
	T (°C)	*S/P*	*R/P*	Pseudo-cube	Cube	Polyhedron	Tetrahedron	Cuboctaedron	Rod	Undefined*
Pt-pseudo cube$_{Sol}$	50	60	1	44	7	0	3	0	2	44
Pt-cube$_{Sol}$	70	5	0.8	44	21		3	4		28
Pt-Mix$_{Sol}$	50	5	1.1		31	54	1	4	3	7
Pt-polyhedron$_{Sol}$	50 + H_2	57	1.4		30	66		3	1	1

* Including aggregates.

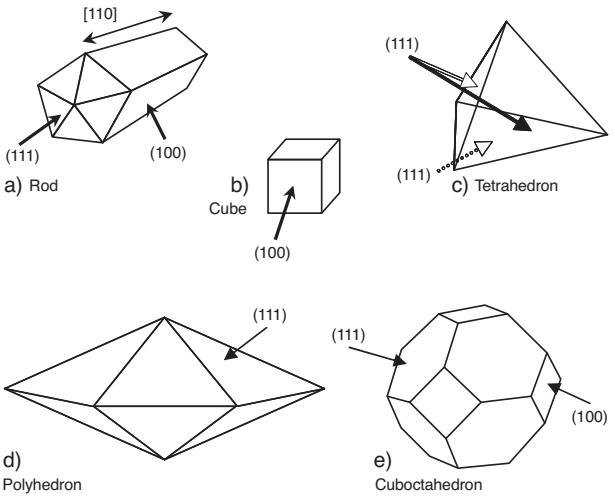

Figure 2

3D modelisations of each type of platinum nanoparticle: a) rod; b) cube; c) tetrahedron; d) polyhedron; e) cubooctahedron.

was also prepared to compare the catalytic properties according to nanoparticle shape. The alumina support was impregnated with an aqueous solution of hydrochloric acid and hexachloroplatinic acid. The support was left in contact with the solution during 24 hours. The catalyst was then dried overnight at 120°C and calcinated in air at 520°C during 2 hours. The catalyst was then treated under air saturated by water at 600°C during 24 hours. This treatment enables the formation of cuboctahedral platinum nanoparticles with an average 6 nm size which is close to the average size of the well faceted platinum nanoparticles prepared in this work.

1.2 Transmission Electron Microscopy

Transmission electron microscopy experiments were performed using a JEOL JEM 2010 apparatus operating at an acceleration voltage of 200 kV. Microscopic analyses were carried out on the platinum nanoparticles in aqueous solution and/or supported on alumina. The platinum solutions were deposited on a perforated carbon film supported by a Cu grid. The grid was then rinsed with ethanol and consecutively dried under an IR light before analysis. The platinum catalysts supported on alumina were crushed in ethanol before deposition on the grid. The frequency distribution is defined by the percentage of each type of platinum of different morphology (cubes, polyhedra, etc.) for a given synthesis procedure. The yield of a type of morphology was calculated as follow:

$$F_i(\%) = \frac{n_i}{n_T}$$

with n_i the number of particles with a given morphology and n_T the number of particles used for the statistical measurement (> two hundred nanoparticles).

1.3 Catalytic Measurements

Buta-1,3-diene hydrogenation was performed in liquid phase using a laboratory scale stainless-steel batch reactor working under static conditions with variation of the concentration of reactant and products over time. Experimental conditions were previously selected in order to avoid mass transfer limitations. Buta-1,3-diene and butenes are hydrogenated following zero order reaction kinetics. One gram of catalyst initially reduced during 2 h under H_2 at 323 K (except $Pt\text{-}Ref_{Cat}$ which was reduced at 773 K) was transferred under Ar in a glove bag into the batch reactor filled with 140 mL of *n*-heptane. The catalyst was then put into contact with 7.0 g of buta-1,3-diene at 293 K under 20 bars of H_2 and high stirring velocity. A pressure gauge before the batch reactor maintains the pressure constant inside the reactor at 20 bars of H_2. The course of the reaction was followed by the loss of H_2 pressure in the pressure gauge and by analysis of samples by gas chromatography (plot alumina column PONA, L = 50 m, split injector; FID detection). The butenes selectivity is defined according to the following equation:

$$\text{butenes selectivity} = \frac{\sum \%(\text{butenes})}{\%(n-\text{butane}) + \sum \%(\text{butenes})}$$

2 RESULTS AND DISCUSSION

2.1 Preparation of Platinum Nanoparticules with Different Morphologies

Different solutions of platinum nanoparticles with different and well defined morphologies are obtained varying the experimental conditions (see *Tab. 1*). The molar CTAB *versus* platinum ratios (defined as *S*/*P*) range from 5 to 60. Molar $NaBH_4$ *versus* platinum ratios (defined as *R*/*P*) varie from 0.8 to 1.4. Preparations have been carried out at 50 or 70°C. The 2D-TEM characterization of each type of obtained platinum nanoparticle is presented Figure 1. The corresponding 3D modelled morphologies deduced from TEM characterizations are defined as follows: cubes, pseudo-cubes, polyhedra, tetrahedra, rods and cuboctahedra and presented Figure 2. The exposed crystallographic planes are deduced for each morphology from the Cubic Face Centered crystallographic structure of platinum and from work previously done for Pd [14]. Cubes (square projection in the 2D-TEM images) expose only the (100) crystallographic plane on each face. Pseudo-cubes are not well crystallized cubes and are supposed to expose the (100) crystallographic plane with a lot of crystallographic defects. Tetrahedra (triangular projection in

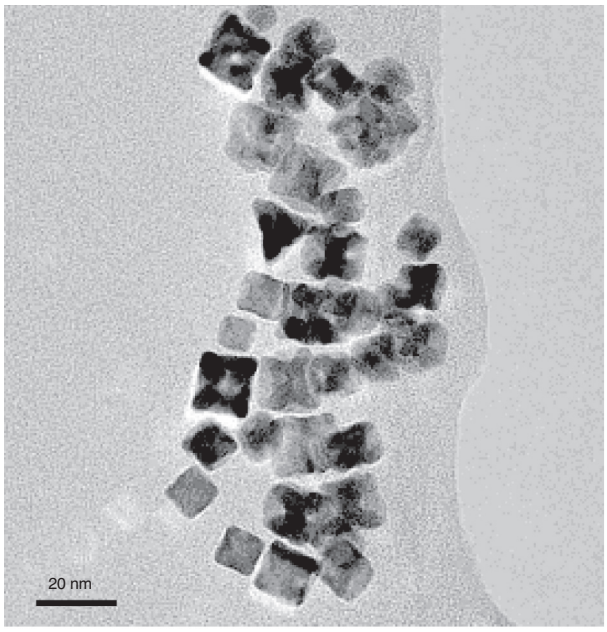

Figure 3

TEM characterization of *Pt-pseudocube*$_{Sol}$ after 3 hours of ageing.

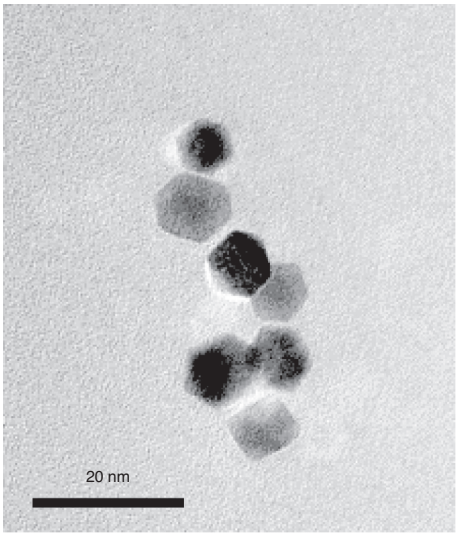

Figure 4

TEM characterization of *Pt-polyhedron*$_{Sol}$ after 3 hours of ageing.

the 2D-TEM images) expose only the (111) crystallographic plane on each face. Rods observed in the 2D-TEM images expose the (100) crystallographic plane on their lateral faces and the (111) crystallographic plane at their extremities. Polyhedra (hexagonal or pentagonal projections in the 2D-TEM images) expose the (111) crystallographic planes [14].

For the *Pt-pseudo-cube*$_{Sol}$ sample (T = 50°C and S/P = 60), mainly platinum nanoparticles with a Pseudo-Cubic morphology (44%) are obtained *(Fig. 3)*. In almost the same conditions, replacement of argon by dihydrogen favours the formation of well crystallized platinum nanoparticles and permits to reach completely different morphologies for the *Pt-polyhedron*$_{Sol}$ sample *(Fig. 4)*, with a majority of well facetted polyhedra (66%), and cubes (30%). The decrease of S/P ratio from 60 to 5 (T = 50°C and S/P = 5) also favours the formation of well crystallized platinum nanoparticles for the *Pt-Mix*$_{Sol}$ sample, since all Pseudo-Cubes have disappeared for this S/P ratio of 5 *(Fig. 5)*. As a consequence, the proportion of well crystallised platinum nanoparticules increases from 12 to 93%. Finally, decreasing the S/P ratio down to 5 and increasing the temperature to 70°C permits to increase the proportion of well facetted cubes for the *Pt-cube*$_{Sol}$ sample up to 21% *(Fig. 6)*. With a constant proportion of pseudo-cubes (44%), the *Pt-cube*$_{Sol}$ sample contains nearly 65% of cubic platinum nanoparticles.

2.2 Study of Platinum Nanoparticles Formation by TEM

The formation of platinum nanoparticles during the *Pt-Mix*$_{Sol}$ preparation was followed by TEM with a time resolved TEM study. Aliquots were periodically sampled (2, 5, 10, 16 min) during the reducing agent injection from the solution and characterized by TEM. Samples of solution were also analyzed during the ageing of the solution after reduction. Platinum nanoparticles formed after 2 min of reducing agent

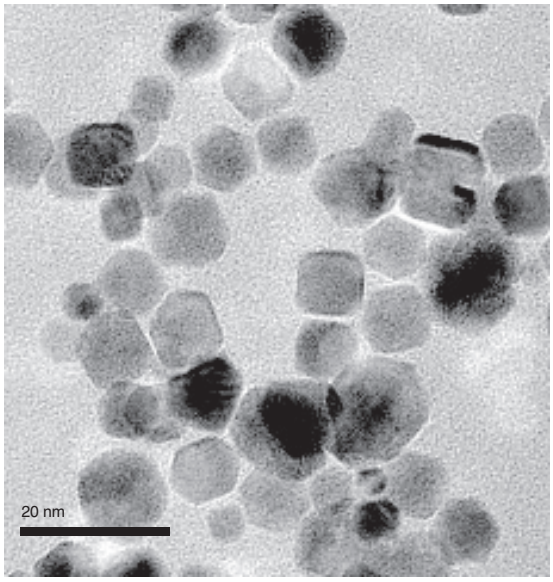

Figure 5

TEM characterization of *Pt-Mix*$_{Sol}$ after 3 hours of ageing.

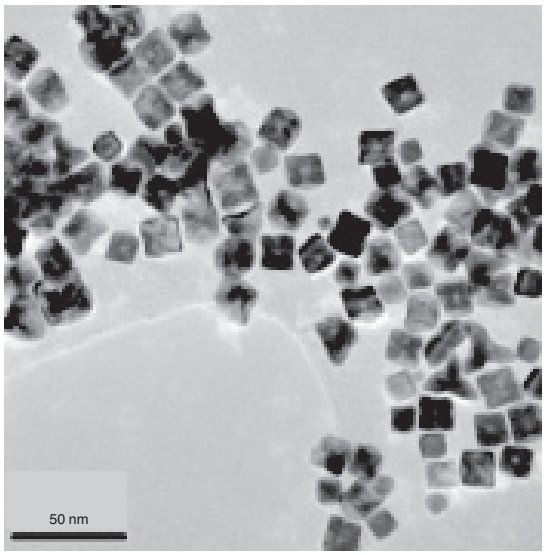

Figure 6

TEM characterization of *Pt-cube*$_{Sol}$ after 3 hours of ageing.

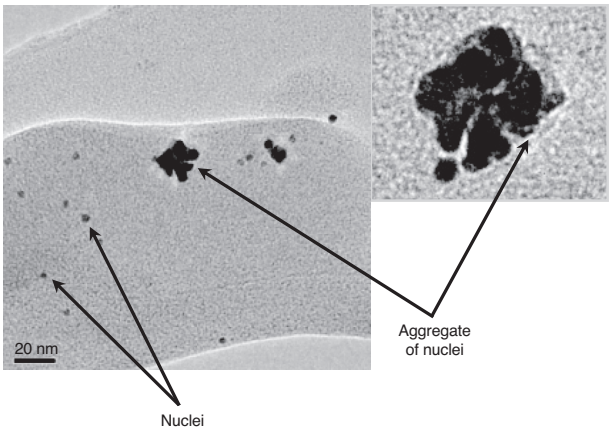

Figure 7

TEM characterization of *Pt-Mix*$_{Sol}$ after 2 min.

injection are presented Figure 7. Nuclei of platinum (almost spherical nanoparticles of nearly 1-5 nm mean size), resulting probably from an homogeneous nucleation process are observed. Theses nanoparticles are present isolated one from each others or aggregated to form aggregates with a size comprised between 10 and 20 nm. Isolated nuclei are present in a large proportion (81%) compared to the proportion of aggregates (17%) (see *Tab.* 2). Platinum nanoparticles formed after 5 min of reducing agent injection are presented Figure 8. The statistical repartition of the observed platinum nanoparticles is completely different. Most of them (90%) are well defined and facetted, as the ones shown Figure 5 after 3 hours of ageing of this *Pt-Mix*$_{Sol}$ sample. The analysis of the size of the cubic nanoparticles shows a mean size of 7-8 nm. Aggregates are still observed but in a less extent (4%). Nuclei almost disappeared (4%). After 16 min of reducing agent injection, the proportion between each type of nanoparticles remains almost constant. Only the size of the well defined cubic single crystals increases, from 7.4 nm at 5 min, up to 10.8 nm at 16 min. And after 16 min, up to 24 hours of ageing under argon atmosphere, there is no further evolution of the nanoparticles in terms of shape, size and even further aggregation.

2.3 Proposition of a Mechanism for Platinum Nanoparticles Formation

Even if the synthesis of metallic nanoparticles (Ag, Au [13], Pd [14, 15]) in aqueous solution was successful, the mechanism of formation of metallic nanoparticles in aqueous solution remains still unclear. Despite the thermodynamic stabilization of given facets by a preferential adsorption of the capping agent can be reasonably considered as the driving force for the controlled growth, other parameters could be also critical to achieve the shape control of the

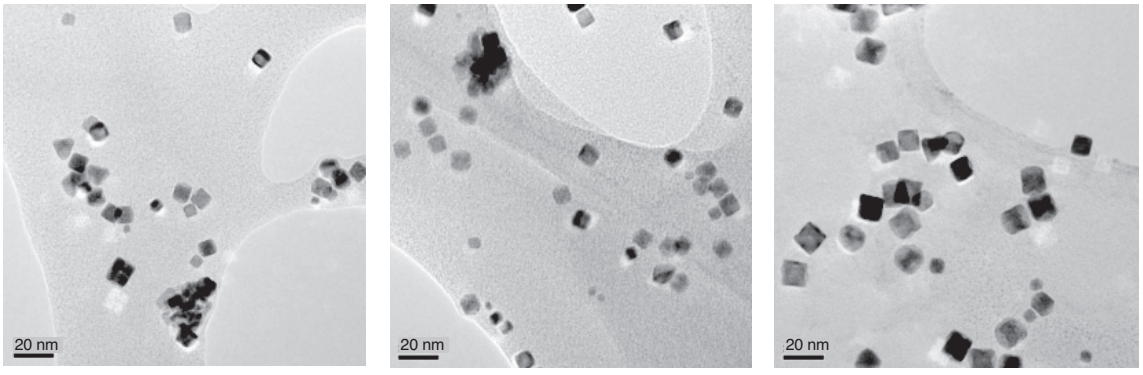

Figure 8

TEM characterization of *Pt-Mix*$_{Sol}$ after 5 a), 10 b) and 16 min c).

TABLE 2

Shapes frequencies of structured platinum nanoparticles deduced from TEM during time resolved TEM measurements

Time of analysis	Proportion in each morphology deduced from TEM (%)				
	Nuclei	Aggregates	Crystallized nanoparticules	Others	Size of cubic crystallized nanoparticles (nm)
2 min	81	17	0	2	/
5 min	4	4	90	2	7.4
10 min	1	4	94	1	9.1
16 min	2	4	93	1	10.8
24 hours	1	5	94	0	11

nanoparticle. In the case of gold, the auto-organization of CTAB molecules in a horizontal bilayer at the surface of the growing particle is supposed to explain the uniaxial growth of gold nanorods through an electric assisted mechanism of molecular growth [34, 35]. A stable Au^{I}-CTAB complex would be formed in solution and reduced to metallic gold directly on the CTAB-embedded metallic surfaces. In the case of palladium, the mechanism of growth seems to be different. The formation of well defined nanoparticles by aggregation of primary particles was evidenced [36]. Concerning platinum, the experimental observations could lead us to suggest a mechanism *(Fig. 9)* for the formation of the platinum nanoparticles.

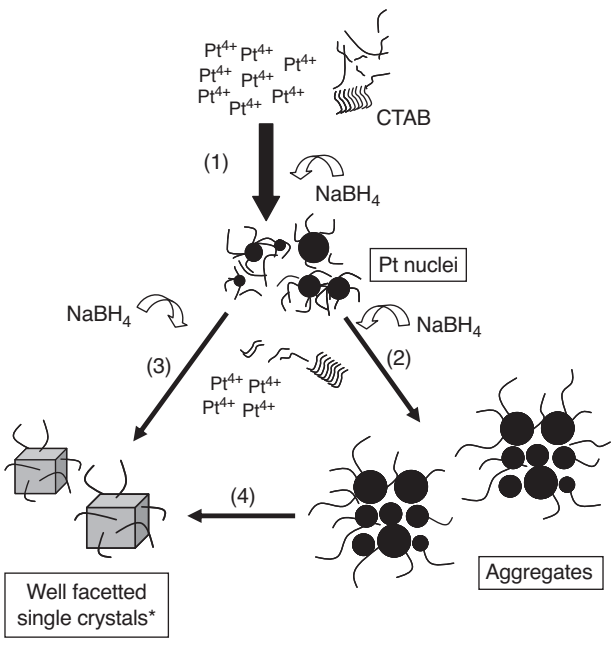

Figure 9

Proposition of a mechanism for platinum nanoparticles formation in solution (* Cubes as an example).

First of all, during the first step (step (1), *Fig. 9*), the platinum salt and CTAB are dissolved in the aqueous solution. CTAB probably forms micellar species since its concentration in solution (around 5 mM in the final solution) is higher than the Critical Micellar Concentration (0.8-1.1 mM) [37]. When the aged H_2PtCl_6 solution is added, the Pt^{4+} cation could be surrounded by different coordination shells since the ageing of the solution is supposed to lead to the partial or complete substitution of chloride ligands by hydroxides ones [21, 22, 38]:

$$[PtCl_6]^{2-} + n\ OH^- \Rightarrow [Pt(OH)_n(Cl)_{6-n}]^{2-} \quad 0 \le n \le 6$$

During step (1), an interaction between CTAB and the platinate salt could be envisaged. Such an interaction could lead to {Pt^{4+}-CTAB} moieties as it was previously demonstrated for palladium [14]. The strong reducing agent, $NaBH_4$, is then injected. It can participate directly to the oxydo-reduction reaction as shown by the following equations:

$$[PtCl_6]^{2-} + 2\ e^- \Rightarrow [PtCl_4]^{2-} + 2\ Cl^- \quad E° = 0.74\ V \quad [39]$$

$$BH_4^- + 3\ H_2O \Rightarrow B(OH)_3 + 7H^+ + 8e^- \quad E° = 0.481\ V \quad [36]$$

$$BH_4^- + 8\ OH^- \Rightarrow H_2BO_3^- + 5H_2O + 8e^- \quad E° = 1.24\ V \quad [36]$$

It can also decompose in solution:

$$NaBH_4 + 2H_2O \Rightarrow NaBO_2 + 4H_2 \quad [40, 41]$$

At the end of step (1), nuclei of reduced platinum, resulting from homogeneous nucleation are thus present and characterized by TEM Figure 7. Theses nuclei are probably capped and stabilized by CTAB.

During step (2), (3) and (4), the injection of reducing agent continues, leading to the formation of aggregates of nuclei ((2)), and well facetted crystals ((3) or (2) + (4)). The mechanism of formation of platinum nanoparticles seems thus to process by an aggregation of primary platinum nanoparticles and coalescence (step (2) + (4)) and/or by a direct molecular reduction of the platinum precursor onto the growing nanoparticle (step (3)). Since well facetted crystals are present in a large proportion (more than 90% after 5 min of reaction), step (3) seems to be preponderant between theses three concomitants steps, in the TEM conditions study.

Referring to the other described preparations, at 50°C and high *S/P* ratio (*S/P* = 60), *Pt-pseudo-cube*$_{Sol}$, 44% of nanoparticles are pseudo-cubes. The coalescence of the primary platinum nanoparticles (step (4)), or direct reduction (step (3)) are thus unfavoured in theses conditions and step (2) becomes predominant. It is well know than CTAB is adsorbed on the surfaces of the nanoparticles [42], so it could hinder coalescence. When the *S/P* ratio is decreased down to 5, *Pt-Mix*$_{Sol}$, a large majority of platinum nanoparticles are well crystallised (93%) and pseudo-cubes have disappeared. Since CTAB is introduced in a lower amount (*S/P* = 5), less CTAB is supposed to be in interaction with the surfaces of the growing nanoparticles and coalescence or/and direct reduction are then favoured. Moreover, at a constant *S/P* ratio (*S/P* = 60), but replacing argon by dihydrogen, *Pt-polyhedron*$_{Sol}$, pseudo-cubes also disappeared and more than 96% of the platinum nanoparticles are well crystallised. A destabilization of the interaction between CTAB and the surfaces of the nanoparticles could be engendered by dihydrogen thus favouring coalescence and/or direct reduction. In theses sets of experimental conditions step (3) and/or (4) seems to be predominant. Moreover, as already discussed in the case of palladium, the destabilisation of the CTAB interaction with the (100) crystallographic plane indirectly favours the most stable platinum (111) surface exposed by polyhedra [43]. Finally, even at a low *S/P* ratio (*S/P* = 5), pseudo-cubes are observed at a temperature of 70°C, *Pt-cube*$_{Sol}$. At such a temperature, homogeneous nucleation is enhanced and the aggregative mechanism (step (2)) is favoured, still leading to the formation of the pseudo-cubes (44%) in front of the well crystallised cubes. We could notice here that at 70°C, cubic nanoparticles thus exposing the (100) crystallographic are predominant (65%). Moreover, temperature seems to favour the existence of the less thermodynamically stable (100) [44] crystallographic plane, when stabilized by CTAB, compared to the (111) crystallographic plane. Platinum nanoparticles are thus formed by two routes in competition, depending on the conditions of synthesis: aggregation (step (2)) and reduction of the platinum precursor on the aggregates thus participating to a coalescence step (step (4)), or direct reduction of the platinum precursor on the surface of the growing nanoparticle (step (3)).

We obtained different kinds of platinum nanoparticles with different morphologies in aqueous solution. Among them, the well crystallized *Pt-Mix*$_{Sol}$ and *Pt-polyhedron*$_{Sol}$ colloidal solutions are good candidates to be deposited on alumina with the aim to prepare model catalysts to study the relationship between morphology (and so the exposed crystallographic plane) and the catalytic properties (selectivity) in a structure sensitive reactions like selective hydrogenation, in the case of platinum.

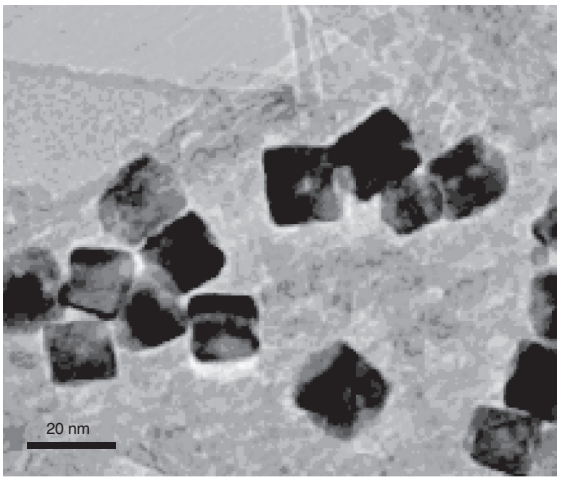

Figure 10

TEM characterization of *Pt-Mix*$_{Cat}$ after deposition of *Pt-Mix*$_{Sol}$ on alumina.

2.4 Preparation of Model Catalysts Containing Well Facetted Platinum Nanoparticles Supported on Alumina

Pt-Mix$_{Cat}$ and *Pt-polyhedron*$_{Cat}$ were prepared by impregnation of the corresponding *Pt-Mix*$_{Sol}$ and *Pt-polyhedron*$_{Sol}$. Their main characteristics are reported Table 3. TEM analyses of the well faceted platinum nanoparticles after deposition on alumina *(Fig. 10)* allowed to verify the influence of the different steps of the deposition procedure (introduction of the alumina powder in the solution, filtration, drying) on morphologies. Due to the support, nanoparticles were difficult to observe by TEM on the supported catalysts, so, no statistical study could be done, as in solution. Nevertheless, morphologies of the supported platinum nanoparticles did not seem to be modified when compared to the morphologies of the platinum nanoparticles in solution.

TABLE 3

Characteristics of the catalysts prepared by deposition of the well faceted platinum nanoparticles

Catalyst	% Pt	Morphology	% (100)*	% (111)*	Undefined
Pt-Mix$_{Cat}$	0.18	Cube-polyhedron	31%	55%	14%
Pt-polyhedron$_{Cat}$	0.16	Polyhedron	30%	66%	4%

* Proportion in (100) and (111) crystallographic planes deduced from shape frequencies determined from MET *(Tab. 1)*.

2.5 Hydrogenation of Buta-1,3-diene Over Alumina Supported Platinum Nanoparticles

An example of the evolution of H_2 consumption and buta-1,3-diene and reaction products (butenes and butane) evolution with time is reported Figure 11 for the *Pt-polyhedron*$_{Cat}$. The evolution of butenes selectivity for *Pt-Mix*$_{Cat}$, *Pt-polyhedron*$_{Cat}$ and *Pt-Ref*$_{Cat}$ catalysts is reported Figure 12. For all catalysts, *n*-butane and butenes are all primary products when buta-1,3-diene is hydrogenated as it is usually the case for platinum [45] which is less selective towards the formation of butenes than palladium for this reaction.

Pt-Ref$_{Cat}$ produces the lowest proportion of butenes whatever the conversion of buta-1,3-diene. However, *Pt-Ref*$_{Cat}$ possesses a high proportion of platinum surface defect atoms. Indeed, considering a cubooctahedron morphology for *Pt-Ref*$_{Cat}$ platinum nanoparticles, their mean diameter of about 6 nm leads to about 20% of surface atoms in corners or edges sites [46]. The proportion of atoms situated on corners and edges for *Pt-Mix*$_{Cat}$ and *Pt-polyhedron*$_{Cat}$ catalysts can also be calculated. Because of their controlled morphologies and their sizes, theses two catalysts expose a minor proportion of surface defect atoms on edges or corners, around 5% +/–2% depending of the type of nanoparticle. *Pt-Mix*$_{Cat}$ which contains nearly 55 % of platinum surface atoms on the (111) crystallographic plane produces more butenes whatever the buta-1,3-diene conversion in comparison with *Pt-Ref*$_{Cat}$. *Pt-polyhedron*$_{Cat}$ which contains a larger proportion of platinum surface atoms on the (111) crystallographic plane (around 66%) produces even higher amounts of butenes. It appears thus clearly than the selectivity towards butenes formation increases when the proportion of platinum surface atoms on the (111) crystallographic plane increases. The presence of platinum (111) surface sites exposed to the reactants seems to contribute to the limitations of the complete hydrogenation towards butane. As a consequence the selective hydrogenation towards butenes is enhanced and favoured.

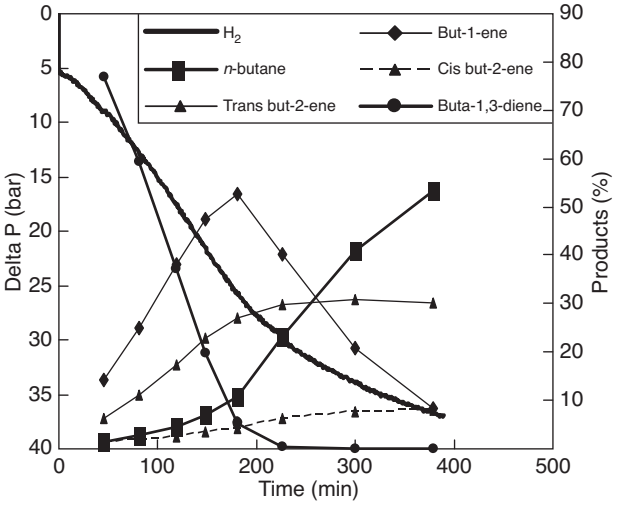

Figure 11

Hydrogenation of buta-1,3-diene (293 K, 20 bars H_2) for *Pt-polyhedron*$_{Cat}$. Evolution of H_2 consumption with time (left axis). Evolution of buta-1,3-diene and reaction products (butenes and n-butane) with time (right axis).

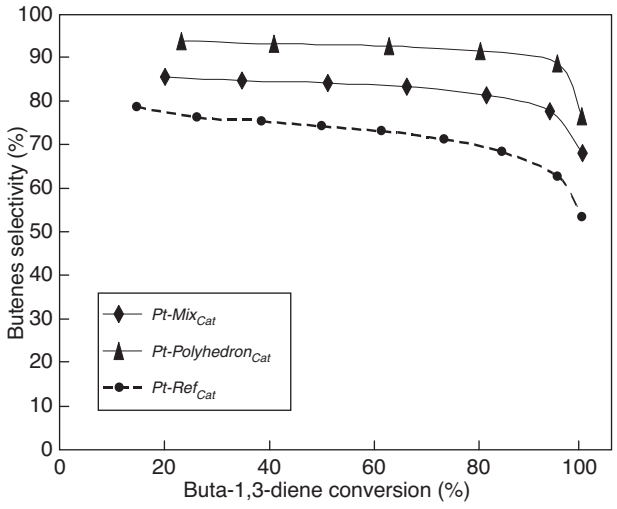

Figure 12

Evolution of butenes selectivity *vs* buta-1,3-diene conversion for *Pt-Mix*$_{Cat}$, *Pt-polyhedron*$_{Cat}$ and *Pt-Ref*$_{Cat}$ catalysts.

CONCLUSION

Platinum nanoparticles with well defined morphologies were successfully prepared in aqueous solution and deposited on an alumina support with no modification of the nanoparticles morphologies. The catalytic properties of the prepared catalysts were studied in the selective hydrogenation of buta-1,3-diene and the link between morphology and selectivity could be established. Catalysts containing a large proportion of platinum surface atoms situated on the (111) crystallographic plane (like *Pt-polyhedron*$_{Cat}$) were highly selective for the hydrogenation of buta-1,3-diene into butenes with a drastic decreasing of the complete hydrogenation to butane.

ACKNOWLEDGMENT

We acknowledge ANR for funding.

REFERENCES

1 Burda C., Chen X., Narayanan R., El-Sayed M.A. (2005) *Chem. Rev.* **105**, 1025-1102.

2 Murphy C.J., Jana N.R. (2002) *Adv. Mater.* **14**, 1, 80-82.

3 Chen S., Carroll D.L. (2004) *J. Phys. Chem. B* **108**, 5500-5506.

4 Tian Z.Q., Ren B., Wu D.Y. (2002) *J. Phys. Chem. B* **106**, 9463-9483.

5 Narayana R., El-Sayed M.A. (2005) *J. Phys. Chem. B* **109**, 12663-12676.

6 Saaski M., Osada M., Higashimoto N., Yamamoto T., Fukuoka A., Ichikawa M. (1999) *J. Mol. Catal. A-Chem.* **141**, 223-240.

7 Boudjahem A.G., Monteverdi S., Mercy M., Bettahar M.M. (2004) *Catal. Lett.* **97**, 177-183.

8 Telkar M.M., Rode C.V., Chaudhari R.V., Joshi S.S., Nalawade A.M. (2004) *Appl. Catal. A-Gen.* **273**, 11-19.

9 Chimentao R.J., Kirm I., Medina F., Rodriguez X., Cesteros Y., Salagre P., Sueiras J.E. (2004) *Chem. Commun.* 846-847.

10 Balint I., Miayazaki A., Aika K. (2004) *Phys. Chem. Chem. Phys.* **6**, 2000-2002.

11 Herricks T., Chen J., Xia Y. (2004) *Nano Lett.* **4**, 12, 2367-2371.

12 Chen J., Herricks T., Xia Y. (2005) *Angew. Chem. Int. Edit.* **44**, 2589-2592.

13 Sau T.K., Murphy C.J. (2004) *J. Am. Chem. Soc.* **126**, 8648-8649.

14 Berhault G., Bausach M., Bisson L., Becerra L., Thomazeau C., Uzio D. (2007) *J. Phys. Chem. C* **111**, 16, 5915-5925.

15 Berhault G., Bisson L., Thomazeau C., Verdon C., Uzio D. (2007) *Appl. Catal. A-Gen.* **327**, 32-43.

16 Balint I., Miyazaki A., Aika K. (2002) *Appl. Catal. B-Environ.* **37**, 217-229.

17 Ahmadi T.S., Wang Z.L., Green T.C., Henglein A., El-Sayed M.A. (1996) *Science* **272**, 1924-1926.

18 Yamada M., Kon S., Miyake M. (2005) *Chem. Lett.* **34**, 7, 1050-1051.

19 Narayana R., El-Sayed M.A. (2004) *J. Phys. Chem. B* **108**, 5726-5733.

20 Narayanan R., El-Sayed M.A. (2004) *J. Am. Chem. Soc.* **126**, 7194-7195.

21 Henglein A., Ershov B.G., Malow M. (1995) *J. Phys. Chem.* **99**, 14129-14136.

22 Henglein A., Giersing M. (2000) *J. Phys. Chem. B* **104**, 6767-6772.

23 Teranishi T., Hosoe M., Tanaka T., Miyake M. (1999) *J. Phys. Chem. B* **103**, 3818-3827.

24 Choo H.P., Liew K.Y., Liu H., Seng C.E., Mahmood W.A.K., Bettahar M. (2003) *J. Mol. Catal. A-Chem.* **191**, 113-121.

25 Chen C.W., Akashi M. (1997) *Langmuir* **13**, 6465-6472.

26 Zhao S.Y., Chen S.H., Wang S.Y., Li D.G., Ma H.Y. (2002) *Langmuir* **18**, 3315-3318.

27 Veisz B., Toth L., Teschner D., Paal Z., Gyorffy N., Wild U., Schlögl R. (2005) *J. Mol. Catal. A-Chem.* **238**, 56-62.

28 Lee H., Habas S.E., Kweskin D.B., Somorjai G.A., Yang P. (2006) *Angew. Chem. Int. Edit.* **45**, 7824-7828.

29 Smith C.E., Biberian J.P., Somorjai G.A. (1979) *J. Catal.* **57**, 3, 426-443.

30 Bertolini J.C., Massardier J., Ruiz P., Tardy B (1989) *Surf. Sci.* **211**, 1053-1060.

31 Narayanan R., El-Sayed M.A. (2004) *Nano Lett.* **4**, 1343-1348.

32 Serrano-Ruiz J.C., López-Cudero A., Solla-Gullón J., Sepúlveda-Escribano A., Aldaz A., Rodríguez-Reinoso F. (2008) *J. Catal.* **253**, 159-166.

33 Bratlie K.M., Lee H., Komvopoulos K., Yang P., Somorjai G.A. (2007) *Nano Lett.* **7**, 10, 3097-3101.

34 Nikoobakht B., El-Sayed M.A. (2001) *Langmuir* **17**, 6368.

35 Perez-Juste J., Liz-Marzan L.M., Carnie S., Chan D.Y.C., Mulvaney P. (2004) *Adv. Funct. Mater.* **14**, 571.

36 Bisson L., Boissière C., Sanchez C., Thomazeau C., Uzio D. (2007) *Mater. Res. Soc. Symp. Proc.* **1017**, DD16-26.

37 Mukerjee P. *et al.* (1971) *Critical Micelle Concentration of aqueous surfactants systems*, NSRDS, pp. 1-226.

38 Zhang F., Chen J., Zhang X., Gao W., Jin R., Guan N., Li Y. (2004) *Langmuir* **20**, 9329-9334.

39 Handbook of chemistry and physics (1982-1983) 63rd ed., CRC press Inc., D-162.

40 Hi S., Brown H.C., Finholt A.E., Gilbreath J.R., Hoekstra H.R., Hyde E.K. (1953) *J. Am. Chem. Soc.* **75**, 215-219.

41 Liu B.H., Li Z.P., Suda S. (2008) *J. Power Sources* **175**, 226-231.

42 Di Gregorio F., Bisson L., Armaroli T., Verdon C., Lemaitre L., Thomazeau C. (2008) *Appl. Catal. A-Gen.* (in press).

43 Bisson L. (2007) *PhD Thesis*, University of Jussieu, France.

44 Vitos L., Ruban A.V., Skriver H.L., Hollar J. (1998) *Surf. Sci.* **411**, 186-202.

45 Bond G.C., Wells P.B. (1964) *Adv. Catal.*

46 Van Hardeveld R., Hartog F. (1969) *Surf. Sci.* **15**, 189.

Final manuscript received in December 2008
Published online in September 2009